Welding Groove Mapping
Implementation and Evaluation of Image Processing Algorithms on Shiny Surfaces

Cristiano Rafael Steffens, Bruno Quaresma Leonardo, Sidnei Carlos da Silva Filho, Valquiria Huttner, Vagner Santos da Rosa and Silvia Silva da Costa Botelho

Federal University of Rio Grande – FURG, Av. Itália – Carreiros – Km 8, 96203–900, Rio Grande, RS, Brazil

Keywords: Robotics, Image Processing, Automation, Welding Robot, Multi-exposure Composition.

Abstract: Electric arc welding is a key process in the heavy steel industries. It is a very complex task that demands a high degree of control in order to meet the international standards for fusion welding. We propose a Vision-Based Measurement (VBM) system and evaluate how different algorithms impact the results. The proposed system joins hardware and software to image the welding plates using a single CMOS camera, run computer vision algorithms and control the welding equipment. A complete prototype, using a commercial linear welding robot is presented. The evaluation of the system as a groove mapping equipment, considering different processing algorithms combined with noise removal and line segment detection techniques, allows us to define the appropriated approach for shop floor operation, combining low asymptotic cost and measurement quality.

1 INTRODUCTION

Welding is a fundamental task in the heavy steel industry. Its automation is required in order to keep pace with the demanding and competitive market. The manual welding process affects directly the quality of the weld - it is very common to have rework due to bad quality welds (Ang Jr et al., 1999). To execute GMAW (Gas Metal Arc Welding) tasks, involving linear steel plates, the welding gun has to perform a longitudinal movement while following the groove between the plates that are being welded. Human operated robots are often used to carry the welding gun. The control parameters of the welding equipment have to be continuously adjusted during the operation. The parametrization demands constant attention and skill of the welding professionals exposing them a harsh and unhealthy conditions.

The overall quality of electric arc welds is highly dependent on the equipment configuration: voltage, current, tractor speed, torch positioning, wire feeding speed and torch weaving, among other parameters. When not properly adjusted, this may result in plate warping, weld spatter, weld slags and fume. Providing a higher level of control for the process is a way to improve the weld quality and avoid rework. It is necessary to implement a system capable of finding the best parameters settings for each welding operation and automate the most critical parts of the process. This can be achieved using algorithmic techniques making the welding process less dependent of the human interaction. In order to achieve this, different techniques can be used depending on the available hardware - sensor and data acquisition system - and cost. We can highlight three main approaches. A combination of structured illumination laser and camera, as used in (Kawahara, 1983), (Drews et al., 1986), (Liu, 2010), (Zhang et al., 2014) and (De Xu, 2004); a touch sensor based approach as in (Kim and Na, 2000) or, a last case, where the arc current feedback is explored, as in (Dilthey and Gollnick, 1998) and (Halmøy, 1999).

The technology has led to a scenario where it is possible to use automated robotic systems to optimize tasks and achieve higher efficiency, productivity and quality, as well as reduce operational costs and rework. Furthermore, the use of robots is recommended for tasks that are taken in hazardous environment or characterize as laborious and repetitive.

Moreover, the advances in both hardware and software technologies enable the development of cheaper, faster, higher quality and smaller cameras and electronic devices. Therefore, vision based methods have become a viable option, combining image acquisition with an operations unit, where algorithms are used to extract useful information. (Shirmohammadi and Fer-

Steffens, C., Leonardo, B., Filho, S., Huttner, V., Rosa, V. and Botelho, S.
Welding Groove Mapping - Implementation and Evaluation of Image Processing Algorithms on Shiny Surfaces.
DOI: 10.5220/0005709103240332
In *Proceedings of the 11th Joint Conference on Computer Vision, Imaging and Computer Graphics Theory and Applications (VISIGRAPP 2016) - Volume 3: VISAPP*, pages 326-334
ISBN: 978-989-758-175-5

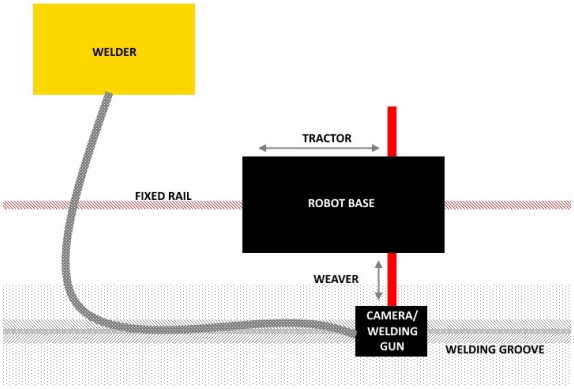

Figure 1: Typical linear welding robot installation.

rero, 2014) argues that, besides the level of automation, Vision-Based Measurement (VBM) is typically faster and more accurate than manual or human based techniques, once it uses electronic devices and computational intelligence.

Imaging a metallic surface, however, is a challenge. This paper proposes a VBM system to recognize the groove geometry for a robotic welding process. Hardware and software are combined to map the welding groove geometry providing the necessary data to adjust the control settings of the welding equipment. A number of alternatives is tested to evaluate the capabilities and impacts of each algorithm choice. Multi-exposure composition is considered as an alternative to obtain non-saturated images of the shiny and reflective surface. The system is implemented on top of a Bug-O Matic Weaver welding robot, manufactured by Bug-O Systems International, using an Altera DE0-Nano FPGA board and a Terasic D5M 5 megapixel camera.

2 LINEAR WELDING ARCHITECTURE

Figure 1 presents a typical setup used on linear welding of thick steel plates employing a welding robot to carry the welding gun. The robot runs on a rail that is fixed to the floor or any other plane surface. The rail is usually parallel to the welding groove that is being welded. The welding equipment is neither a part nor is it dragged by the robot. In a typical scenario, the robot is solely used to drag the welding gun with controlled speed an weaving.

Depending on the groove properties (see Figure 2), the weaver and tractor are combined to produce different weld patterns (a.k.a Oscillation Regime):

- Continuous: the robot travels continuously over the rail both during weave and dwell;

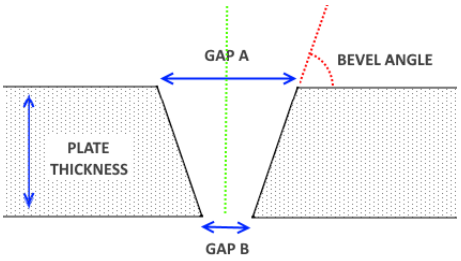

Figure 2: Welding groove properties.

- Step: the robot travels only during dwell, and stops during the Weaver cross stroke;
- Tractor Stop on Dwell: robot travels on the rail during weave stroke. Tractor and Weaver stop during dwell;
- Line or Stringer Bead: weaver is turned off;

In our approach, a lighting system and camera equipment are attached to the welding gun mounting point. The robot control is mapped and modified to enable an automated control of the tractor and weaver, allowing us to adjust the camera position while the robot travels over the entire rail, and thus map the welding groove properties.

3 A VISION BASED APPROACH FOR WELDING GROOVE MEASUREMENT

A VBM system usually consists of a visual sensor plus operations unit (Figure 3 gives an overview of the VBM system). The visual sensor can be a camera, laser scanner, x-ray scanner, or any other sensor which an image of the physical scene containing the measurand can be obtained, and the operations unit can be implemented in software or hardware (Shirmohammadi and Ferrero, 2014).

3.1 Image Aquisition

Figure 4 gives an overview on the proposed image acquisition setup. Proper choice of lighting, camera and lens are keys to any successful VBM system design. For our application, they become even more important once the steel or iron plates can present both specular and diffuse reflection and the amount of light that is reflected is also highly affected by the plate oxidation or dust. Therefore, a lighting system has been designed to enhance the groove properties. It uses an arrangement of LEDs (Light-Emitting Diode) positioned beside the camera.

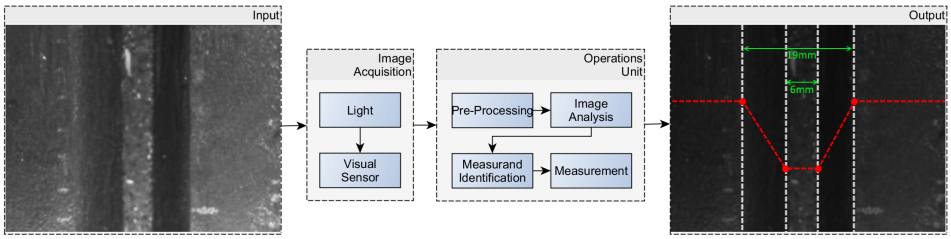

Figure 3: High-level architecture of a Vision-Based Measurement system.

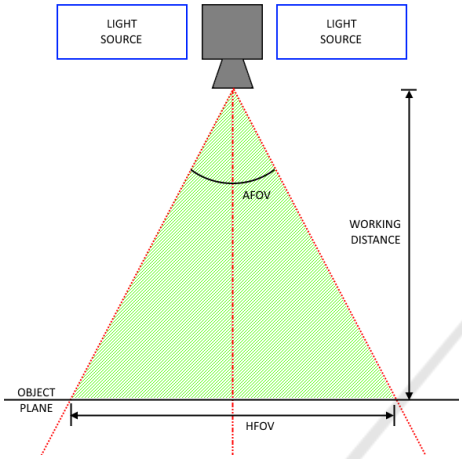

Figure 4: Image Acquisition setup.

On a pinhole camera, assuming that a fixed working distance will be ensured on the setup steps, the Horizontal Field of View is given by Eq. 1, where WD is the distance from the lens front principal plane to the object plane and $AFOV$ is the Angular Field of View of the lens.

$$HFOV[mm] = 2 \cdot WD \cdot tan\left(\frac{AFOV[^\circ]}{2}\right) \quad (1)$$

The lens experiences greater magnification as the object distance from the lens changes. Since the top and bottom faces of the welding plate have a different WD the pixel to metric unit conversion has to consider that difference when computing the groove width and bevel angle. The scale factor S is given by Eq. 2, where d_{object} is the physical dimension of a given object in millimeters and d_{image} is the size of the correspondent object on the image in pixels.

$$S[mm/pixel] = \frac{d_{object}}{d_{image}} \quad (2)$$

Raw data is obtained from the Bayer-filter CMOS sensor and converted to a grayscale image. Metallic surfaces introduce some difficulties that are not yet resolved in the literature. They differ from standard rigid structured, non-reflective surfaces that computer vision usually deals with. Slight changes on the illumination, camera movement, parent material oxidation or dust often produce extreme differences in radiance values that are impossible to capture without either under-exposing or saturating the sensor. Standard image processing operations expect pixel values to be proportional to the scene radiance. Due to nonlinear image response these operations often produce incorrect results for conventional images. Therefore, from this point, taking advantage of the low level control provided by the customised hardware, we have tested two different alternatives for the image acquisition.

1. Single frame capture using fixed exposure time: a exposure time that is at the center of the range the camera supports is used. It provides reasonable visibility of the details in the scene for most cases. The image is normalized and the histogram is equalized.
2. Multi-exposure image composition: The exposure time is controlled to obtain k images of the exact same place. Multi-exposure composition, as proposed in (Debevec and Malik, 2008), is used to obtain a High Dynamic Range (HDR) image. The HDR image is latter normalized to a 2^8 range, so it can be used as input on standard image processing techniques as they are implemented in OpenCV 3.0. On the same hand, normalizing the pixel values to a lower range also works as a low pass filter, removing noisy pixels.

3.2 Operations Unit

The proposed system uses image processing and machine vision to detect the welding groove's properties. The groove is modeled as a set of almost parallel lines on the image. As the system is implemented in hardware, the algorithms must be carefully selected to maximize the accuracy and performance levels.

3.2.1 Noise Removal

We apply a gaussian unsharp mask to enhance the high frequency regions present at the groove edges.

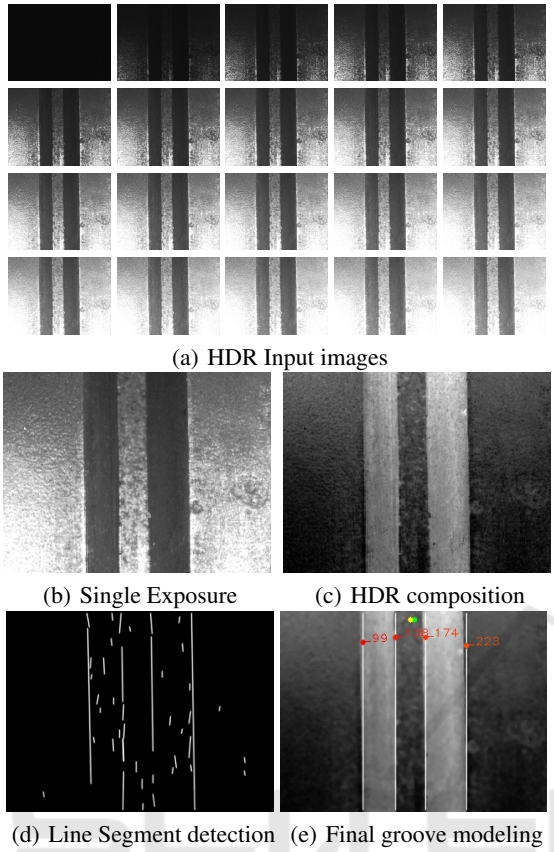

(a) HDR Input images

(b) Single Exposure (c) HDR composition

(d) Line Segment detection (e) Final groove modeling

Figure 5: Processing in the VBM system.

While it improves the overall contrast, it also accentuates the small failures and aberrations that are already on the captured image. Therefore, a noise removal step is necessary. For the noise removal step test three filters: a mean box filter, a median filter and a gaussian filter. Gaussian and mean filters have a linear computational complexity, but both of them work as low-pass filters, which might be a drawback given that edges perform an important rule on the groove detection. The classic median filter has a $O(n\log(n))$ complexity, once, by definition it requires the pixels in the neighbourhood to be ordered by their value. Optimized approaches, as presented in (Perreault and Hébert, 2007), can bring it down to $O(n)$.

3.2.2 Straight Line Detection

The camera position is orthogonal to the observed surface. Once the image is preprocessed we can now work on the line detection to determine the groove properties. Among previous approaches that focus on standardized computer vision algorithms, such as (Ma et al., 2010), (Hou and Liu, 2012) and (Xu et al., 2012), the combination of a Canny edge detector and a Hough transform is the most recurrent alternative. In order to identify the straight lines the Hough transform associates to each pixel on a input image, in a polar geometry space, to the bundle of lines passing through it.

However, as we intend to implement the machine vision step on a low cost equipment with real-time performance, we have to consider the algorithms complexity and use a solution that maximizes the asymptotic cost/ output quality ratio. Although it is non-deterministic, it has been evidenced in (Risse, 1989) and latter in (Hollitt, 2009) that the computational cost of the Canny edge detection plus the cost of the classical Hough line transform can be over $O(n^4)$, where n is the number of pixels in the analysed image. Using some simplification steps, authors were able to reduce the complexity down to $O(n^3 \log n)$ (Hollitt, 2009), which we believe is still not appropriated for the system restrictions. Besides its complexity, the Canny edge detector also depends on predefined threshold values. Therefore, four alternative algorithms were evaluated:

- PPHT – Progressive Probabilistic Hough Transform for Line Detection (Galamhos et al., 1999): It is non-deterministic like the standard Hough transform itself. Considering its enhanced voting scheme we tested it expecting it to be less susceptible to random noise.
- Fast LSD (Von Gioi et al., 2012): LSD works with gray scale images detecting lines formed by edges. The LSD was designed with the intention of not requiring parameters adjustment. It has a $O(n\log(n))$ asymptotic complexity.
- EDLines (Akinlar and Topal, 2011): It is parameterless and has a $O(n\log(n))$ asymptotic complexity. It works upon the Edge Drawing algorithm (Topal et al., 2010) that uses Sobel gradient filters to replace the classic Canny filters.
- LSWMS – Line Segment Detection Using Weighted Mean Shift (Nieto et al., 2011): Designed to detect line segments in real-time applications, the algorithm has a $O(n)$ complexity. Authors agree it generates noisy results, but recommend it for application like vanishing point detection because it provided enough accuracy and great speed.

3.2.3 Heuristics

Once we know the possible groove edges, a greedy Non-Maximum Suppression algorithm is used to separate false positives and negatives that still remain after the image processing. To determine the point that better represents the groove edges on the image,

the endpoints of the line segments are interpolated and combined to form a histogram of the aggregated values in the image row axis. Using the application domain information we can establish some threshold values to filter the outputs of the vision algorithms. For instance, it is known the steel plates thickness can vary from 13mm up to 20mm and groove angle can vary within 45-55°. Also a restriction of the application domain, the Gap B, on the plate bottom, has to be something between 3mm and 9mm. Pixel to millimeter conversion and world position association achieved via encoder based dead-reckoning complete the mapping, supporting the decision making and welding equipment actuation.

4 IMPLEMENTATION

The VBM system has been implemented as a module to replace the original Control Unit of the BUG-O modular system. The digital system features a FPGA based hardware/software architecture. The main goal of using a FPGA system instead of a standard computer is the customization level and integration of the hardware/software solution that can be obtained. The DE0-Nano board, manufactured by Altera Corporation, was chosen due to their low cost, high number of logic cells and digital I/O pin count, integrated flash memory, RAM, and 12-bit A/D conversion. Furthermore the DE0-Nano is pinout compatible with the D5M camera module, simplifying the electronic design. The electronic interfaces were developed using low cost off-the-shelf integrated and discrete components for signal conditioning.

Both the image acquisition system and the welding torch are mounted on the end-effector of the robot. A Terasic D5M camera is used for image acquisition. It features a single package containing sensor and lens. Table 1 shows its specification considering a full resolution image capture according to the manufacturer. Once we crop the image for our application, the angular field of view is reduced in the same ratio.

A LED illumination circuit has been created to provide an adequate homogeneous illumination and minimize the influence caused by changes of ambient light. For the image acquisition a CMOS camera has been used. The operations unit, as well as the light control and image acquisition, is implemented on the FPGA development board , which is responsible for receiving the image acquired by the visual sensor, performing the image processing and the adjustment of the robot's and welder's parameters in real time.

The raw data acquisition and basic image processing are performed on the FPGA board taking advantage of the embedded Altera's Nios® II processor. A SDRAM memory is used to create a frame buffer. The image is sent, without compression, to a standard PC via Universal Asynchronous Receiver/Transmitter (UART) and a USB FTDI breakout port. Camera and robot control instructions are sent via Modbus RTU serial communication protocol with 921600 of baudrate. Noise suppression and straight line detection steps are executed on a C++ OpenCv version 3.0 based software. We use the code made available by the authors for the LSWMS algorithm and Fast LSD. The EDLines algorithms is implemented "in house" since the authors do not make it publicly available. Non-maximum suppression and heuristics are used to identify the welding groove parameters. The processed data is then used to control the robot and welder.

Table 1: Terasic D5M Sensor and Optics Specification.

Specification	Value
Sensor Active Array Size	2592 x 1994
Image Size	5.7mm(H) x 4.28mm(V)
Pixel Size	2.2μm x 2.2μm
Focal Lenght	7.12mm
Fixed Aperture	F/3.25 ($\pm$ 5%)
Angular Field Of View	55°
Relative Illumination	$\geq$ 65.0%
Barrel Distortion	$\leq$ 1.0%

The system is integrated with a reliable and widely accepted industrial robot. Encoders are used as odometer sensors (dead reckoning) of the tractor and weaver arm. The data is decoded using an 8-bit quadrature decoder module designed in VHDL. Both tractor and weaver speed setpoints are calculated using a $\Delta\Sigma$ module with 12 bit resolution.

A Lincoln Electric Flextec™ 450 Multi-Process Welder is used. It is able to perform stick, DC TIG, MIG, Flux-Cored, Arc Gouging welds. For our application, the original user interface is replaced to use the digital input provided by the VBM system. A sample of the relationship between the grove geometry and the equipment controls is shown in Table 2. These settings have been carefully defined by welding specialists at Mitsubishi Heavy Industries. The oscillation regime defines the behaviour of the pendulum extension and the weaving amplitude. Depending on the groove properties it can require up to 4 layers of weld. Electrode diameter, electrode extension and gun position are predefined by the welder. The oscillation regime (OR) is a preset that combines the robot's tractor and weaver, with a specific speed and distance, to result in different weld patterns.

An overview of the digital control system is shown in Figure 6. The central controller is the main unit in the system. All the tasks involving the control and

Table 2: Sample of the geometry to welder control mapping. Legend: PT – Plate Thickness [mm]; G – Gap B; B^o – Bevel Angle [^{o}]; WS – Weld Speed [mm/min]; TS – Tractor Speed [%]; LH – Layer Height [mm]; OR – Oscillation regime; WF – Wire Feed Speed [m/min]; A – Current [A].

Groove Prop.			Equipment Settings						
PT	G	B^o	L	WS	TS	LH	OR	WF	A
13	3	45	1	450	64	3	a	14	6.2
			2	340	49	5	a	14	6.2
			3	330	75	3	b	14	6.2
			4	320	75	3	b	14	6.2

Table 3: Compilation report.

Specification	Description	Used
FPGA Device	EP4CE22F17C6	–
Total Logic Elements	5.916	27%
Combinational Functions	5.380	24%
Dedicated logic registers	3.152	14%
FPGA PLLs	1/4	24%
I/O pins (external)	96	62%
Embedded Multiplier 9-bit	0	0%
Total memory bits	42.992	7%

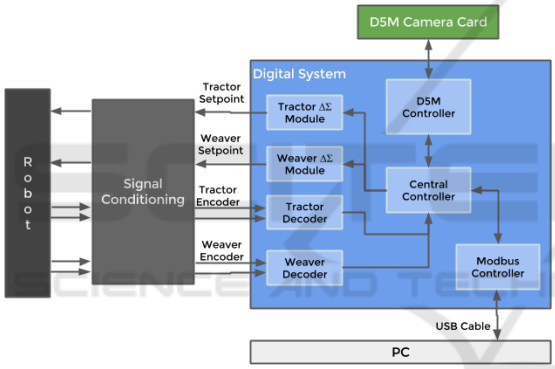

Figure 6: Overview of Digital Control System.

parametrization of the camera, sending or receiving data via modbus and ΔΣ module are controlled in this component. The execution order is to read all the data signals from the decoders and read any message driven from the modbus component, based on that take actions such as start or stop the camera acquisition or move the robot using the tractor or weaver ΔΣ module. The project is designed in Altera's development platform tool Quartus II. The compilation report presented in Table 3, showing the relative occupation of its resources.

5 EXPERIMENT RESULTS

The proposed VBM system is evaluated as a measuring equipment considering both measurement error and measurement uncertainty. According to the GUM (BIPM et al., 2008), the purpose of a measurement is to determine the value of the measurand, i.e., the value of the particular quantity to be measured. A complete measurement is taken by an appropriate specification of the measurand, the method of measurement, and the measurement procedure. Generally, the result of a measurement is only an approximation or estimate of the value of the measurand and thus is complete only when accompanied by a statement of the uncertainty of that estimate.

Table 4: Measurement Evaluation. Values in millimeters. Lower error and standard deviation is better.

	$\bar{E}$ A	σ A	$\bar{E}$ B	σ B
Gauss + EDLines	0.407	0.370	1.071	0.407
Mean + EDLines	0.340	0.383	0.961	0.739
Median + EDLines	0.344	0.290	1.002	0.505
Gauss + LSWMS	1.204	2.197	0.933	0.797
Mean + LSWMS	0.367	0.389	0.842	1.134
Median + LSWMS	1.548	2.640	1.066	1.123
Gauss + PPHT	12.053	10.312	4.506	2.657
Mean + PPHT	0.424	0.392	1.225	0.417
Median + PPHT	3.267	6.380	1.559	1.304
Gauss + Hough	19.916	0.000	6.558	0.000
Mean + Hough	17.963	6.176	5.976	1.838
Median + Hough	16.001	8.470	5.429	2.391
Gauss + LSD	0.143	0.084	0.780	0.157
Mean + LSD	0.306	0.298	0.902	0.380
Median + LSD	0.241	0.257	1.056	0.442
HDR + Gauss + EDLines	1.110	2.249	1.327	0.670
HDR + Mean + EDLines	0.359	0.399	0.731	0.505
HDR + Median + EDLines	0.254	0.190	0.912	1.188
HDR + Gauss + LSWMS	1.586	2.406	0.678	0.680
HDR + Mean + LSWMS	1.119	1.945	0.970	0.772
HDR + Median + LSWMS	1.511	2.299	0.912	0.800
HDR + Gauss + PPHT	19.916	0.000	6.558	0.000
HDR + Mean + PPHT	0.242	0.112	0.763	0.296
HDR + Median + PPHT	0.294	0.228	1.054	0.780
HDR + Gauss + Hough	19.916	0.000	6.558	0.000
HDR + Mean + Hough	17.920	6.327	5.908	2.054
HDR + Median + Hough	10.107	10.346	3.618	3.105
HDR + Gauss + LSD	0.358	0.388	0.985	0.420
HDR + Mean + LSD	0.364	0.355	0.697	0.477
HDR + Median + LSD	0.345	0.302	0.782	0.485

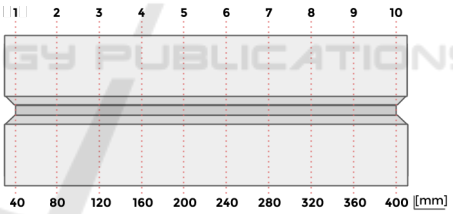

Figure 7: Groove unit separation in 40mm each.

The groove is measured using a caliper rule with three digits decimal precision, at a temperature of 20° Celsius. A 400mm specimen is used to obtain 10 sample points, separated 40mm from each other as shown in Fig. 7. The robot is programmed to follows the groove stopping at each sample point. At each position a image is acquired and processed using 30 combinations of noise removal filters and line

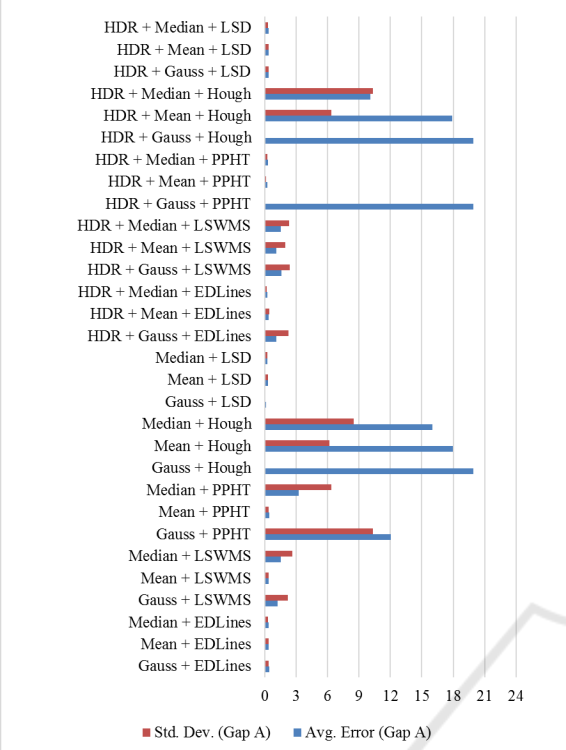

Figure 8: Average error and standard deviation of the measured values on the top of the plate (Gap A). Values in millimeters.

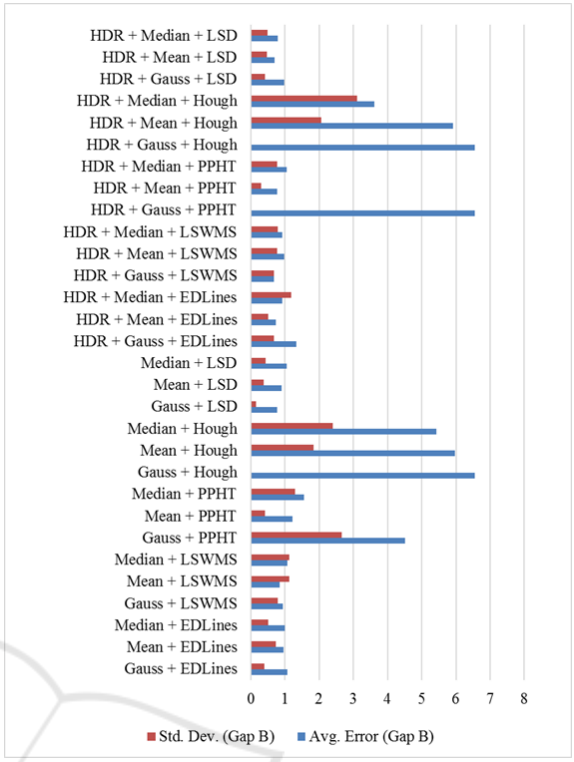

Figure 9: Average error and standard deviation of the measured values on the bottom of the plate (Gap B). Values in millimeters.

segment detection algorithms. The task is completed after the entire plate is mapped. It is important to note that the samples 6, 7, 8, and 9 where obtained on a recently polished part, which consequently presents more specular reflection.

We used a 5 pixels kernel for all the noise suppression filters. The gaussian filter uses a 0.7 standard deviation. The Canny minimal an maximal threshold values are set to 100 and 200 respectively. The Hough transform uses a L_1 norm. On images were one of the lines failed to be detected, Gap A and Gap B were considered as 0. Fig. 8 shows the Gap A (plate top) values measured by the VBM system for the 10 samples of the welding plate. Fig. 9 shows the Gap B (plate bottom) values measured for the same samples.

Table 4 allows us to compare the ground truth with the VBM system measurements, showing the average value and distribution. The combination of median blur and EDLines line segment detection shows the smallest standard deviation. On the other hand, Gaussian combined with EDLines presents the smallest error.

Based on the data we can state that, for these sample points, Fast LSD algorithm provides the best results. Using any of the noise suppression kernels its standard deviation is still lower than the other tested combinations on both Gap A and Gap B measurements. The next best solutions, which minimize error and standard deviation are obtained using the EDLines algorithm. As third position in the rank, LSWMS also presents a low error, but depending on the noise suppression choice, its standart deviation can go over two millimeters.

It is important to note that both classic Hough Transform and its variant PPHT perform worse than the others. The combination of Gaussian kernel with the classic Hough transform fails in all sample points. Other classic Hough combinations also fail in many of the processed images. In this sense, PPHT shows a significant improvement. When combined with the mean filter, it presents a very low standard deviation, becoming a suitable option given that systemic error can be easily compensated. It is important to note that the Canny thresholds are a user input. Varying them to get proper edge detection for each test point image would improve the results, but that is not a viable option when developing an automated solution.

Furthermore, the results also show the HDR composition does not significantly increase the output quality. Although it reduces the standard deviation in most cases, it increases the average error. That is a unexpected behaviour, once we could expect the vi-

sually improved images to perform better due to the absence of saturated and underexposed regions.

Evaluating the combinations we can also make some assumptions about the relation within filters and line detectors. Fast LSD and EDLines are little affected by the kernel choices. In both single exposure images and multi-exposure composed images, the results change less than 100 nanometers. LSWMS is affected by the filter type when applied to HDR images. Hough and PPHT, in the other hand, are highly affected by the filter choice. Using a Gaussian low pass filter reduces the detection rate, making the detector fail in all cases. The median filter, also increases error and variation, making the mean filter the best option.

Finally, the experiment results show that, even though it is widely used in academic research, the Hough transform can be replaced by modern, state-of-the-art algorithms, improving both detection quality and computational complexity bounds.

6 CONCLUSIONS AND FUTURE WORK

We present a system that integrates different techniques to perform dimensional measurement of thick steel plate bevels. We show how, using domain knowledge, the extracted dimensions can be mapped in control settings for the robotic welding equipment. Unlike the previous approaches, it does not rely on a single moving spot like laser trackers, nor a pattern of spots like optical contact systems, neither a line like laser scanners. No structured light or polarized lenses are used. The approach is based on image acquisition and processing making use of computer vision algorithms. The groove modeling is achieved through the use of line detection algorithms that look for straight lines and segments. State-of-the-art algorithms, such as Debevec's HDR composition, Fast LSD, PPHT, LSWMS and EDLines were tested on real data to evaluate their capabilities.

Experimental results demonstrated that, using carefully selected algorithm combinations, the system can successfully extract the measurand dimensions. The proposed approach has evident advantages over the manual process that is used in shop floor nowadays, given that it can yield a large number of features in a very short time using state of the art algorithms, is not susceptible to the most frequent measurement error sources and automatically controls the welding equipment settings. In the same hand, we also demonstrated obsolete and non-deterministic algorithms could be replaced by state-of-the art alternatives achieving better results at lower computational cost.

We will be further exploring lighting options, noise suppression algorithms and image composition techniques to test how the achieved results can be improved to surpass the precision requirements of the welding industry. Previous studies have shown the impact of illumination wavelength on enhancing or suppressing desired properties on the image surface. We believe it might also impact the image acquisition on reflective surfaces. On the same hand, bilateral filtering and image smoothing via L0 gradient minimization (Xu et al., 2011), which have not been tested yet due to their computational complexity bounds and inability to perform in real-time on the proposed hardware architecture, will be included in the comparison. Furthermore, Debevec's multi-exposure image composition will be compared to other recent approaches that minimize the computational cost and are hardware-friendly.

In the long term, machine learning and deep learning will be used to extract information of the process and produce a general purpose welding workcell. Therefore it must be able to identify the material and it's conditions; the environment variables such as wind and humidity and incorporate the knowledge that only experienced weldors today have. Studies have already been realized to map the main differences among senior and novice weldors and we intend to use them to elevate the overall quality of the welding process.

ACKNOWLEDGEMENTS

This work was supported by National Counsel of Technological and Scientific Development (CNPq), Coordination for the Improvement of Higher Education Personnel (CAPES) and Funding Authority for Studies and Projects (FINEP).

REFERENCES

Akinlar, C. and Topal, C. (2011). Edlines: A real-time line segment detector with a false detection control. *Pattern Recognition Letters*, 32(13):1633–1642.

Ang Jr, M. H., Lin, W., and Lim, S.-Y. (1999). A walk-through programmed robot for welding in shipyards. *Industrial Robot: An International Journal*, 26(5):377–388.

BIPM, I., IFCC, I., ISO, I., and IUPAP, O. (2008). Evaluation of measurement data – guide to the expression of uncertainty in measurement.

De Xu, Min Tan, X. Z. Z. T. (2004). Seam tracking and visual control for robotic arc welding based on struc-

tured light stereovision. *International Journal of Automation and Computing*, 1(1):63.

Debevec, P. E. and Malik, J. (2008). Recovering high dynamic range radiance maps from photographs. In *ACM SIGGRAPH 2008 classes*, page 31. ACM.

Dilthey, U. and Gollnick, J. (1998). Through the arc sensing in gma-welding with high speed rotating torch. In *Industrial Electronics Society, 1998. IECON'98. Proceedings of the 24th Annual Conference of the IEEE*, volume 4, pages 2374–2377. IEEE.

Drews, P., Frassek, B., and Willms, K. (1986). Optical sensor systems for automated arc welding. *Robotics*, 2(1):31–43.

Galamhos, C., Matas, J., and Kittler, J. (1999). Progressive probabilistic hough transform for line detection. In *Computer Vision and Pattern Recognition, 1999. IEEE Computer Society Conference on.*, volume 1, pages –560 Vol. 1.

Halmøy, E. (1999). Simulation of rotational arc sensing in gas metal arc welding. *Science and Technology of Welding & Joining*, 4(6):347–351.

Hollitt, C. (2009). Reduction of computational complexity of hough transforms using a convolution approach. In *Image and Vision Computing New Zealand, 2009. IVCNZ'09. 24th International Conference*, pages 373–378. IEEE.

Hou, X. and Liu, H. (2012). Welding image edge detection and identification research based on canny operator. In *Computer Science & Service System (CSSS), 2012 International Conference on*, pages 250–253. IEEE.

Kawahara, M. (1983). Tracking control system using image sensor for arc welding. *Automatica*, 19(4):357–363.

Kim, C. H. and Na, S. J. (2000). A study on rotating arc using hollow shaft motor. *Journal of Korean Welding Society*, 18:589–594.

Liu, X. (2010). Image processing in weld seam tracking with laser vision based on radon transform and fcm clustering segmentation. *ICICTA*, pages 470–473.

Ma, H., Wei, S., Sheng, Z., Lin, T., and Chen, S. (2010). Robot welding seam tracking method based on passive vision for thin plate closed-gap butt welding. *The International Journal of Advanced Manufacturing Technology*, 48(9-12):945–953.

Nieto, M., Cuevas, C., Salgado, L., and García, N. (2011). Line segment detection using weighted mean shift procedures on a 2d slice sampling strategy. *Pattern Analysis and Applications*, 14(2):149–163.

Perreault, S. and Hébert, P. (2007). Median filtering in constant time. *Image Processing, IEEE Transactions on*, 16(9):2389–2394.

Risse, T. (1989). Hough transform for line recognition: complexity of evidence accumulation and cluster detection. *Computer Vision, Graphics, and Image Processing*, 46(3):327–345.

Shirmohammadi, S. and Ferrero, A. (2014). Camera as the instrument: the rising trend of vision based measurement. *Instrumentation & Measurement Magazine, IEEE*, 17(3):41–47.

Topal, C., Akınlar, C., and Genç, Y. (2010). Edge drawing: a heuristic approach to robust real-time edge detection. In *Pattern Recognition (ICPR), 2010 20th International Conference on*, pages 2424–2427. IEEE.

Von Gioi, R. G., Jakubowicz, J., Morel, J.-M., and Randall, G. (2012). Lsd: a line segment detector. *Image Processing On Line*, 2(3):5.

Xu, L., Lu, C., Xu, Y., and Jia, J. (2011). Image smoothing via l 0 gradient minimization. In *ACM Transactions on Graphics (TOG)*, volume 30, page 174. ACM.

Xu, Y., Yu, H., Zhong, J., Lin, T., and Chen, S. (2012). Real-time seam tracking control technology during welding robot gtaw process based on passive vision sensor. *Journal of Materials Processing Technology*, 212(8):1654–1662.

Zhang, L., Ke, W., Ye, Q., and Jiao, J. (2014). A novel laser vision sensor for weld line detection on wall-climbing robot. *Optics & Laser Technology*, 60:69–79.